ChemPubSoc Europe

DOI: 10.1002/ejic.201600917

EurJIC European Journal of Inorganic Chemistry

Full Paper

Electrocatalytic Ni Complexes

Nickel Complexes of Pyridine-Functionalized N-Heterocyclic Carbenes: Syntheses, Structures, and Activity in Electrocatalytic Hydrogen Production

Siyuan Luo,[a] Maxime A. Siegler,[b] and Elisabeth Bouwman*[a]

Abstract: Two bis(benz)imidazolium salts alkylated with pyridyl side arms, H_2**L1**Br_2 (1,2-bis{[1-(2-pyridylmethyl)benzimidazolium-3-yl]methyl}benzene bromide) and H_2**L2**Br_2 (1,2-bis-{[1-(2-pyridylmethyl)imidazolium-3-yl]methyl}benzene bromide) have been prepared and were used as precursors in the synthesis of novel nickel compounds of N-heterocyclic carbenes (Ni-NHCs). The four Ni-NHC complexes [Ni(**L1**)Br]Br (**1a**), [Ni(**L1**)]$(PF_6)_2$ (**1b**), [Ni(**L2**)]Br_2 (**2a**) and [Ni(**L2**)]$(PF_6)_2$ (**2b**) were isolated and characterized by various methods, and the X-ray crystal structures of **1a**, **2a** and **2b** are reported. The nickel ion in **1a** is in a square-pyramidal geometry with one of the bromide ions in the apical position, the nickel ions in **2a** and **2b** are in square-planar geometries. The compounds of the ligand with an imidazole-based carbene revealed much higher activity in electrocatalytic proton reduction and better acid tolerance, although their overpotentials are higher than those of the benzimidazole-based compounds. The presence of bromide ions has an adverse effect on the redox potentials as well as the overpotentials for proton reduction. Complex **2b**, having the most planar coordination geometry, appeared to have the highest catalytic efficiency for proton reduction in DMF (i_c/i_p = 50, k_{obs} = 490 s^{-1} at 0.1 V/s) when using acetic acid as the proton source. To the best of our knowledge, this is the first report of Ni-NHC complexes that are active in electrocatalytic proton reduction.

Introduction

Dihydrogen is an environmentally friendly energy carrier as upon combustion it only produces H_2O.[1,2] In order to enable the establishment of a society based on dihydrogen as an energy source, for many years researchers have focused on the search for efficient proton-reduction catalysts, notably for catalysts that are not based on noble metals.[3–7] In the field of bioinorganic chemistry the synthesis of structural models of hydrogenases is a common strategy to devise molecular catalysts for proton reduction.[8,9] However, the so-called "functional models" of hydrogenases, which do not exhibit exactly similar structures, appear to result in more active and more stable catalytic systems. The two-electron donor ligands such as phosphanes and amines have been widely used in combination with Co[10–12] and Ni[7,13] metal centers. The N-heterocyclic carbene (NHC) ligand is also a two-electron donor, with strong binding properties comparable to that of phosphane ligands.[14] Although Ni-NHC complexes have found various applications in organometallic chemistry,[15–21] the electrocatalytic properties of this kind of compounds so far mostly have been neglected.

NHC ligands functionalized with pyridine groups have been used to synthesize nickel and palladium complexes that were found to be efficient catalysts for the Kumada cross-coupling[22] and Heck-type coupling reactions.[23] Recently, the group of Kubiak reported a study of nickel compounds with four carbene ligands including their electrochemical characterization, but their activity in electrocatalysis was not discussed.[24] A series of nickel complexes with NHC-pyridine ligands was reported by Thoi et al.[25,26] to selectively reduce carbon dioxide to carbon monoxide. Nevertheless, the number of studies in the area of electrocatalysis using Ni-NHC compounds is limited. Herein, we report four novel Ni-NHC complexes obtained with the ligand precursors H_2**L1**Br_2 and H_2**L2**Br_2, which are based on bis(benz)imidazolium salts bridged by a xylyl linker (Scheme 1).

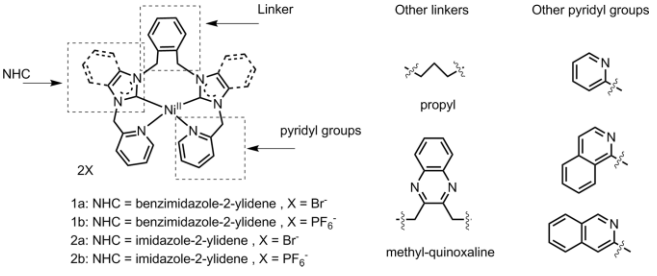

Scheme 1. Complexes reported in this paper (linker = xylyl) and related compounds previously reported (with linker = propyl[26] or methylquinoxaline[27]).

[a] *Leiden Institute of Chemistry, Gorlaeus Laboratories, Leiden University, P. O. Box 9502, 2300 RA Leiden, The Netherlands*
E-mail: bouwman@chem.leidenuniv.nl
http://mcbim.lic.leidenuniv.nl/
[b] *Department of Chemistry, Johns Hopkins University, 3400 N. Charles Street, Baltimore, Maryland 21218, USA*
Supporting information and ORCID(s) from the author(s) for this article are available on the WWW under http://dx.doi.org/10.1002/ejic.201600917.

We have studied their redox properties and electrocatalytic activity for proton reduction in an organic solvent.

Results and Discussion

Syntheses

The two bis(benz)imidazolium salts 1,2-bis{[1-(2-pyridylmethyl)benzimidazolium-3-yl]methyl}benzene bromide (H_2**L1**Br_2) and 1,2-bis{[1-(2-pyridylmethyl)imidazolium-3-yl]-methyl}benzene bromide (H_2**L2**Br_2) were synthesized following published procedures with small modifications.[28,29] The nickel bromide compounds [Ni(**L1**)Br]Br (**1a**) and [Ni(**L2**)]Br_2 (**2a**) were obtained as yellow-colored powders from a melt of nickel acetate with the ligand in tetrabutylammonium bromide (TBAB) in good yields (74 and 55 %, respectively). The color of complex **1a** turned to orange once dried under vacuum overnight. Whereas the benzimidazole-based complex **1a** is poorly soluble in water, the imidazole-based compound **2a** is soluble in water. Compounds [Ni(**L1**)]$(PF_6)_2$ (**1b**) and [Ni(**L2**)]$(PF_6)_2$ (**2b**) were obtained from **1a** and **2a** via anion exchange by adding a solution of the complex in methanol to a boiling methanol solution of NH_4PF_6. All complexes are air and moisture stable in the solid state for at least several months. The low-spin character of the Ni^{II} ion in all compounds is evidenced by their diamagnetic ^{1}H NMR spectra, indicating that the square-planar geometry of the Ni centers is retained in solution. The ESI-MS analysis of the four compounds shows the presence of monocationic (with one coordinated bromide anion, or as an ion pair) as well as dicationic fragment ions. Recrystallized samples of the Ni compounds were dried in vacuo before elemental analysis was performed; however, in some cases the analysis still showed the presence of the solvents used in recrystallization.

Single Crystal X-ray Crystallography

Single crystals of **1a**, **2a**, and **2b** suitable for X-ray diffraction were obtained using the liquid-liquid diffusion method (MeCN/diethyl ether). The crystallographic data are provided in Table 1, selected bond lengths and bond angles are given in Table 2.

Table 2. Selected bond lengths (Å) and angles (°) of compounds **1a**, **2a**, and **2b**.

	1a	2a	2b
Ni1–N22	1.962(2)	1.946(7)	1.942(3)
Ni1–N52	1.963(2)	1.929(2)	1.932(3)
Ni1–C12	1.879(2)	1.877(5)	1.879(4)
Ni1–C42	1.882(2)	1.876(3)	1.887(4)
Ni1–Br2	3.080(8)		
N22–Ni1–C12	87.42(9)	87.29(3)	87.8(2)
N22–Ni1–C42	176.72(9)	171.7(3)	172.7(1)
N22–Ni1–N52	87.86(8)	86.5(3)	89.4(1)
C12–Ni1–C42	95.8(1)	99.1(2)	95.0(2)
C12–Ni1–N52	171.03(9)	167.7(2)	173.4(2)
C42–Ni1–N52	88.86(9)	88.2(1)	88.5(1)

Compound **1a** crystallizes as a monocationic complex with one uncoordinated bromide ion and 1.5 water molecules per asymmetric unit. The nickel ion in complex **1a** is coordinated in a square-pyramidal geometry, with the donor atoms of the tetradentate ligand in the equatorial plane and one coordinating bromide ion at the apical position (Figure 1). The bond length to the apical bromide (Ni1–Br2) is 3.0800(8) Å. This distance is rather long and could be considered as a normal van der Waals contact; however, also the coordination angles (between 86–99°), the small torsion angle of the equatorial plane and the low τ_5 value (see below) are indicative of a stronger interaction. The tetradentate ligand is wrapped around the nickel ion with the aromatic groups orientated in a zig-zag fashion with respect to each other. The ligand donor atoms form an approximate plane with only a small torsion angle [N22–N52–C42–C12 = 5.18(8)°], with Ni–N and Ni–C bond lengths in the range of 1.882–1.963 Å, consistent with the typical distances reported for this type of structures.[21,27] The N–Ni–C and C–Ni–C bond angles are slightly smaller than the ideal right angles (87.42–88.86°), but the "open" N52–Ni1–N22 angle is slightly larger [95.85(9)°]. The five-coordinate geometry is char-

Table 1. Selected crystallographic and structure refinement data for complex **1a**, **2a** and **2b**.

	1a	2a	2b
Empirical formula	$C_{34}H_{28}BrN_6Ni$, (Br), 1.5(H_2O)	$C_{26}H_{24}N_6Ni$, 2(Br), 2.361(H_2O), 0.431(O)	$C_{26}H_{24}N_6Ni$, 2(PF_6)
Formula weight	766.18	688.50	769.16
Temperature (K)	110(2)	110(2)	110(2)
Crystal system	monoclinic	monoclinic	monoclinic
Space group	*C2/c*	*C2/c*	$P2_1/c$
a (Å)	36.2037(12)	32.8374(6),	23.0500(14)
b (Å)	11.2404(2)	8.89992(13)	9.5940(3)
c (Å)	16.7135(6)	20.2657(4)	14.7070(7)
β (°)	109.865(4)	109.610(2)	105.683(6)
V (Å^3)	6396.7(4)	5579.13(18)	3131.3(3)
Z	8	8	4
D_{calc} (g/cm^3)	1.591	1.639	1.632
μ (mm^{-1})	3.145	4.65	2.796
F(000)	3096	2777	1552
Crystal size (mm)	0.27 × 0.17 × 0.10	0.26 × 0.09 × 0.02	0.25 × 0.14 × 0.01
Reflections collected, unique, $I > 2\sigma(I)$	25476, 7345, 6196	23382, 5423, 4625	18755, 6111, 5006
R-factor, $I > 2\sigma(I)$	R_1 = 0.0290, wR_2 = 0.0635	R_1 = 0.0298, wR_2 = 0.0761	R_1 = 0.0698, wR_2 = 0.1823
R-factor (all data)	R_1 = 0.0400, wR_2 = 0.0674	R_1 = 0.0372, wR_2 = 0.0810	R_1 = 0.0832, wR_2 = 0.1933
$\Delta\varrho_{max}$, $\Delta\varrho_{min}$ (e Å^{-3})	0.43, –0.49	0.61, –0.56	0.92, –0.71

acterized with a τ_5 value of 0.09, indicating that the nickel ion is coordinated in a near ideal square pyramid.[30]

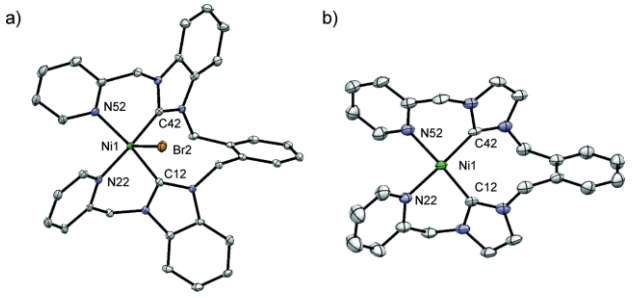

Figure 1. Displacement ellipsoid plots (50 % probability level) of the cations: a) [Ni(**L1**)Br]$^+$ in **1a** and b) [Ni(**L1**)]$^{2+}$ in **2b** at 110(2) K. Atom numbering scheme for the first coordination sphere is provided. Hydrogen atoms, the non-coordinated bromide ion, the hexafluoridophosphate ion and the lattice water molecules are omitted for clarity.

The five-coordinate geometry of the nickel ion in **1a** is not rare; five-coordinate geometries can be divided into two categories: the trigonal bipyramid[31] and the tetragonal pyramid.[32] The square-pyramidal geometry is commonly formed with pentadentate chelating ligands,[33] or from a combination of tridentate and bidentate chelating ligands.[34,35] Square-pyramidal structures formed by a tetradentate ligand with an additional halide ion are rather rare.[36,37] The non-coordinating bromide ion and the lattice water molecules are connected with the coordinating bromide ion via hydrogen bonding interactions.

Compounds **2a** and **2b** crystallize as dicationic complexes with the non-coordinating bromide ions and the solvent molecules (**2a**) or the hexafluoridophosphate ions (**2b**) in the crystal lattice. The nickel ion in these complexes is coordinated in a square-planar geometry, with the donor atoms of the tetradentate ligand wrapped around the nickel ion (Figure 1). The Ni–N bond lengths in **2a** and **2b** are slightly shorter than those in **1a** (see Table 2), whereas the Ni–C bond lengths are rather similar.

The square-planar geometry of the nickel ion in **2a** was evaluated with an equation[24] derived from a report by Yang.[38] The largest and second-largest L–Ni–L angles in **2a** are 171.7(3)° and 167.7(2)°, resulting in a τ_4 value of 0.06. For compound **2b** a τ_4 value of 0.04 is calculated, indicating that the geometry of the central ion in both compounds is close to the ideal square-planar geometry. The structures of the nickel(II) compounds have been compared with those earlier reported (Table 2 and Table S1);[26] it appears that ligands containing pyridylmethyl pendant arms result in longer Ni–C bond lengths compared to ligands with pyridyl side groups. The donor atoms of tetradentate ligands containing the more flexible pyridylmethyl groups are arranged in a more planar fashion around the nickel ions with lower τ_4 values (τ_4 = 0.09 for pyridylmethyl groups and 0.14 for pyridyl groups). The different linkers in the dicarbene chelating structure may also affect the planarity of the arrangement of donor atoms around the nickel centers: Ligands with rigid linkers containing an aromatic group such as xylene (**2a** τ_4 = 0.06; **2b** τ_4 = 0.04) or dimethylquinoxaline[27] (τ_4 = 0.03) generally present smaller τ_4 values than the ligands with alkyl linkers (τ_4 = 0.12–0.14, see Table S1).[26]

UV/Vis Absorption Studies

Electronic absorption spectra of the four nickel compounds as well as the precursor ligands H_2**L1**Br_2 and H_2**L2**Br_2 were recorded both in the solid state and in DMF solutions (see Table 3 and Figures S2–S5).

The solid-state absorption spectra of the ligand precursors H_2**L1**Br_2 and H_2**L2**Br_2 show one absorption around 260 nm ascribed to π–π* transitions of the pyridyl groups.[39] The absorption bands in the solid-state spectrum of **1a** at 305 and 355 nm are assigned to ligand-to-metal charge-transfer (LMCT) transitions, and the absorption at 433 nm is assigned to a d-d transition (Figure S3). Similar assignments are proposed for the spectra of the other compounds (Figure S4).

Compounds **2a**, **1b** and **2b** readily dissolve in dry DMF resulting clear (pale) yellow solutions (within 1 min). However, the solubility of **1a** is lower, initially resulting in a cloudy solution; only after stirring for 1 h the solution became clear. The limited solubility of **1a** in DMF may be related to the coordination of one of the bromide ions; perhaps only upon dissociation of this bromide ion the compound is fully soluble. The UV/Vis spectra in DMF again show the intense π–π* transition of the pyridyl groups at around 275 nm and an intense transition around 310 nm, which has been ascribed to a ligand-to metal charge transfer (LMCT of carbene to nickel).[40] All compounds show a d-d transition in the region of 360–380 nm common for square-planar nickel(II) complexes (Figure S5).

Electrochemical Studies

Electrochemical analysis of the four nickel complexes in dry DMF was performed with 0.1 M tetrabutylammonium hexafluoridophosphate (TBAP) as the supporting electrolyte under a stream of argon. An Ag/AgCl reference electrode was used, but the potentials are reported vs. the ferrocene/ferrocinium ($Fc^{0/+}$)

Table 3. Parameters of the electronic spectra of Ni complexes and ligands.

	Solid state optical spectra [nm]	Absorption bands, λ_{max} nm (ε/M^{-1} cm^{-1})[a]
1a	264, 305, 355, 433 sh	276 (4640), 311 (5230), 361 sh (1170)
1b	262 298, 324, 390	280 (4450), 314 (5860), 389 sh (360)
2a	260, 308, 351	274 (4000), 305 (4860), 378 sh (510)
2b	258, 299, 384	273 (2860), 307 (3860), 381 sh (180)
H_2L1Br_2	259	275 (4750)
H_2L2Br_2	258	267 (4000)

[a] The spectra were recorded in DMF at 22 °C at a concentration of 1 mM.

couple, which was added after each experiment. The electrochemical data of the nickel compounds are collected in Table 4.

Table 4. Electrochemical data of the nickel compounds.[a]

	E_{pc1} [V]	E_{pa1} [V]	$E_{1/2}$ [V] (ΔE_p [mV])	E_{pc2} [V]	E_{pa2} [V]	$E_{1/2}$ [V] (ΔE_p [mV])	E_{pc3} [V]
1a	–1.59	–1.51	–1.55 (82)	–1.84	–1.76	–1.80 (79)	–2.04
1b	–1.58	–1.49	–1.53 (84)	–1.80	–1.72	–1.76 (80)	–2.00
2a	–1.76	–1.67	–1.71 (82)	–1.96	–1.86	–1.91 (100)	–2.27
2b	–1.70	–1.63	–1.66 (75)	–1.90	–1.82	–1.86 (84)	–2.23

[a] All voltammograms were recorded in DMF; the potentials are referenced to the $Fc^{+/0}$ couple. Conditions: scan rate = 0.1 V/s, compound (1 mM), TBAP (0.1 M), glassy-carbon working electrode. Under these conditions we found ΔE_p ($Fc^{+/0}$) = 78 mV.

The cyclic voltammogram of complex **1a** shows the presence of three reductive waves, two of which are reversible (see Figure 2). The two reversible waves are tentatively assigned to the Ni^{II}/Ni^{I} and Ni^{I}/Ni^{0} redox couples ($E_{1/2}$ = –1.55 and –1.80 V). However, the formation of a Ni^{I} species with a ligand-centred radical is also possible, although the voltammogram of the ligand does not have a reduction wave coinciding with the second reversible reduction of the complex. Without a full spectroelectrochemical study the true nature of the reduction process occurring at –1.8 V is unknown. The first reversible redox wave at –1.55 V vs. $Fc^{0/+}$, is characterized by a peak current ratio i_{pa}/i_{pc} of 0.99. A plot of the reductive peak current i_{pc} displays a linear relationships with the square root of the scan rate (Figure S6), which demonstrates this first electrochemical reduction to be diffusion-controlled.[41] In addition, the current also increases linearly with the concentration of the nickel compound (Figure S7). The third small reductive peak at –2.04 V is tentatively attributed to a ligand-based process, forming a ligand-centered radical, as its position coincides with a reduction wave observed in the CV of H_2**L1**Br_2 (see Figure 2).

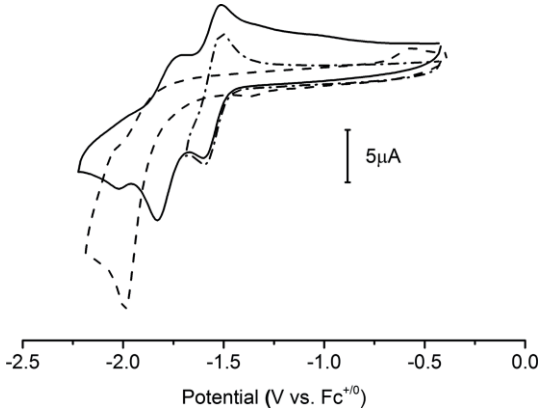

Figure 2. Cyclic voltammograms of **1a** (1 mM, solid line and dash-dotted line) and H_2**L1**Br_2 (1 mM, dashed line) recorded in DMF in different scan ranges. Conditions: scan rate: 0.1 V/s, TBAP (0.1 M), glassy-carbon working electrode.

Compound **2a** reveals a similar cyclic voltammogram with three reduction processes at –1.76, –1.96 and –2.27 V, and two oxidation processes at –1.67 and –1.86 V. However, the redox processes are significantly less reversible; the peak-current ratio i_{pa}/i_{pc} of the first reduction event is 0.75 indicating a quasi-reversible redox process (Figure S8). The voltammograms of the hexafluoridophosphate species **1b** and **2b** show similar patterns compared to their bromide analogs, but with the redox processes occurring at less negative redox potentials (by about 20–50 mV); the presence of the potentially coordinating anions apparently stabilizes the Ni^{II} oxidation state.

It appears that the nickel compounds with a benzimidazole-based carbene ligand are more readily reduced with less negative half-wave potentials (–1.53 V, –1.55 V) than those with the imidazole-based carbenes (–1.66 V, –1.71 V), indicating the imidazole-based ligands to be slightly more electron-donating. The redox potentials of these nickel compounds with the relatively hard pyridyl ligands occur at rather negative potentials compared to Ni centers that are coordinated with softer phosphane ligands.[13,32]

Catalytic Activity for Proton Reduction in Non-Aqueous Solution

The four compounds have been investigated for their catalytic activity in the electrocatalytic proton reduction in DMF, using either acetic acid (HOAc) or trifluoroacetic acid (Htfa) as the proton source. For each scan the working electrode was freshly polished.

When using the strong acid Htfa as the proton source (pK_a in DMF: 6.0[42]), two new reductive waves (–1.9 and –2.4 V) appeared after two irreversible peaks at –1.6 and –1.8 V (Figure 3), which is consistent with the report of Canaguier et al.[6] The catalytic current i_c is the maximum current of the catalytic proton-reduction peak, and i_p is the plateau current of the non-catalytic reduction waves. The current of this catalytic wave is dependent on the acid concentration, but saturates at a concentration of 40 mM. As shown in Figure 3 and Figure S9, the i_c/i_p ratio increases linearly with the acid concentration until the acid-independent region is reached. This saturation indicates that at this acid level the main rate-controlling process is no longer acid diffusion, but rather the catalytic efficiency of the Ni complex. The i_c/i_p value is 13 in the acid-independent region (at a scan rate of 0.1 V/s) which corresponds to a rate constant (k_{obs}) of 33 s^{-1}.[7,43]

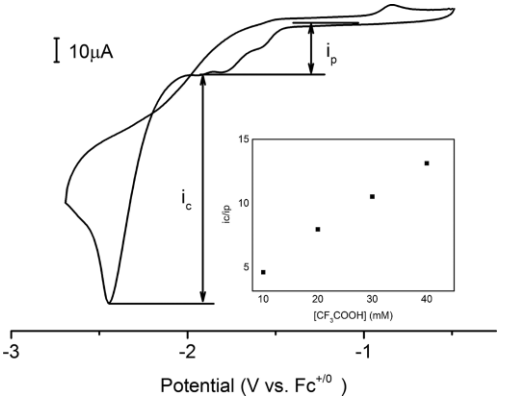

Figure 3. Cyclic voltammogram of **1a** (1 mM) in presence of Htfa (10 mM) recorded in DMF. Conditions: scan rate: 0.1 V/s, TBAP (0.1 M), glassy-carbon working electrode. Inset: plot of i_c/i_p vs. [Htfa]. The value for i_c is the maximum current of the catalytic peak, and i_p is the plateau current of the non-catalytic wave, as indicated in the Figure.

Activity for proton reduction is also observed when the weaker acetic acid is added to a solution of **1a** in DMF. The two reversible redox couples as well as the third irreversible reductive wave combine into one irreversible wave at –1.8 V. Meanwhile only one new reduction peak is observed at –2.6 V. The current of this peak is dependent on the acid concentration and thus is ascribed to the electrocatalytic reduction of protons by the nickel compound. The appearance of bubbles on the GC working electrode during the experiment is another visible indication for H_2 production. No obvious current enhancement is observed in a blank experiment using the same quantity of acid in the absence of nickel complex (see Figure S10).

Comparison of the catalytic activities of four Ni complexes using acetic acid as the proton source, showed the i_c/i_p value of compound **2b** to be highest, reaching 50 (corresponding to $k_{obs} = 490^{-1}$ at 0.1 V/s) at an acid concentration of 80 mM (Figure 4, Figure S11 and Table 5). The overpotential of the four molecular catalysts for electrocatalytic proton reduction at an acetic acid concentration of 10 mM has been calculated taking homoconjugation of the acid into account (Table 5).[44] Imidazole-based compound **2b**, the most efficient electrocatalyst of the four compounds, unfortunately displays a higher overpotential (1.28 V) than the benzimidazole-based carbene complexes (ca. 1.15 V). Furthermore, the presence of bromide ions in complexes results in slightly higher overpotentials (30–50 mV difference).

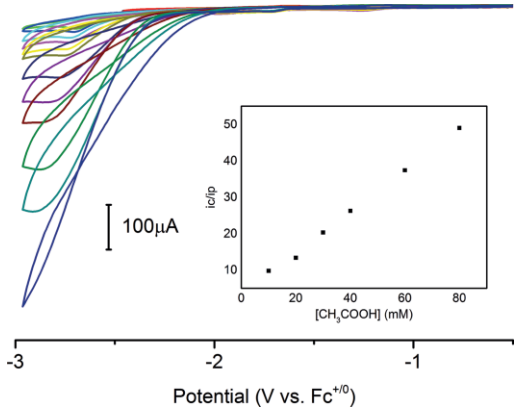

Figure 4. Cyclic voltammograms of 1 mM solutions of **2b** with various amounts of acetic acid (0–120 equiv.) in 0.1 M TBAP-DMF at 0.1 V/s. Inset: plot of i_c/i_p vs. [CH_3COOH] for **2b**.

Table 5. Summary of the electrocatalytic properties of the compounds.[a]

	1a	1b	2a	2b
[HOAc] (mM)	16	16	80	80
i_c/i_p	5.4	4.5	35	50
k_{obs}	5.7	4.0	240	490
Overpotential (V)[b]	1.17	1.14	1.33	1.28

[a] The i_c/i_p value, k_{obs} and overpotentials of the reductive waves of the four complexes(1 mM) at the maximum concentration of acetic acid at a scan rate of 0.1 V/s (vs. $Fc^{+/0}$). [b] Overpotentials of complexes were calculated in the presence of 10 mM acetic acid.

Conclusions

In this paper we report four novel pyridine-functionalized Ni-NHC complexes and their redox and electrocatalytic properties. The linker type between the carbenes as well as the bridge to the pyridine group influences the geometry of the complexes, as characterized by their τ_4 values. It appears that a rigid linker based on an aromatic group in combination with a pyridylmethyl pendent group attributes to more ideal square-planar geometries. We found that the use of imidazole-based carbenes result in much higher catalytic activity for electrocatalytic reduction of protons, as well as better acid tolerance, although these compounds reveal more negative Ni^{II}/Ni^{I} and Ni^{I}/Ni^{0} redox couples and higher overpotentials. The most planar complex **2b** (with the smallest τ_4 value) shows the highest catalytic efficiency (i_c/i_p = 50, $k_{obs} = 490^{-1}$at 0.1 V/s) of all complexes investigated in this study for the catalytic proton reduction using acetic acid, although the overpotential at which dihydrogen is produced is sizeable. To the best of our knowledge, these are the first Ni-NHC complexes reported to catalyze proton reduction. Only a few recent reports relate to proton reduction with metal-NHC compounds, but these concern cobalt-NHC complexes.[14,45]

Furthermore, it was shown that the presence of halide ions results in more negative potentials for the Ni^{II}/Ni^{I} and Ni^{I}/Ni^{0} redox couples, and also leads to larger overpotentials for proton reduction.

The experiments of catalytic proton reduction in organic solvents provide a starting point for analysis; however, water is the ideal solvent for H_2 production. Considering the higher solubility of the hexafluoridophosphate salts in aqueous solutions and the adverse effect of the bromide ions on the catalytic activity of the nickel compounds, further investigations to proton reduction catalysis with this type of molecular catalysts will be carried out in acid-buffered aqueous solutions. Although the observed overpotentials are not outstanding, the reported nickel compounds are attractive: the synthesis route of the complexes is straightforward and the complexes are air and moisture stable due to the presence of the bis-carbene donor. Based on their ease of synthesis and overall stability this type of molecular catalysts may thus be competitive with the diimide/phosphane Ni catalysts.

Experimental Section

General: Commercial chemicals and solvent were used without further purification. Dry solvent obtained from PureSolv MD5. All air-sensitive reactions were performed under argon using standard Schlenk techniques unless mentioned otherwise.

^{1}H, ^{13}C and ^{31}P NMR spectra were recorded on a Bruker 300 DPX spectrometer. Mass spectra were obtained using a Finnigan Aqua Mass Spectrometer (MS) with electro spray ionization (ESI). UV/Vis spectra were obtained using either a transmission dip probe or a solid-state reflection probe on a Avantes Avaspec-2048 spectrometer with a Avalight-DH-S-BAL light source. Elemental analyses were performed by the Kolbe Mikroanalytisches Laboratorium, Germany.

X-ray Structural Determination: All reflection intensities were measured at 110(2) K using a SuperNova diffractometer (equipped with Atlas detector) with Mo-K_α radiation (λ = 0.71073 Å) (**1a**) or Cu-K_α radiation (λ = 1.54178 Å) (**2a**, **2b**) under the program CrysAlisPro

(version 1.171.36.32 Agilent Technologies, 2013). The same program was used to refine the cell dimensions and for data reduction. The structure was solved with the program SHELXS-2013[46] and was refined on F^2 with SHELXL-2013.[46] Analytical numeric absorption corrections based on a multifaceted crystal model were applied using CrysAlisPro. The temperature of the data collection was controlled using the system Cryojet (manufactured by Oxford Instruments). The H atoms were placed at calculated positions (unless otherwise specified, see below) using the instructions AFIX 23 or AFIX 43 with isotropic displacement parameters having values 1.2 times U_{eq} of the attached C atoms.

1a: The H atoms attached to O1W and O2W (i.e., lattice water molecules) were found from difference Fourier maps, and their coordinates were refined freely. The structure is ordered. The crystal lattice also contains some amount of very disordered solvent molecules. Their contribution has been taken out using the SQUEEZE procedure[47] in the final refinement (SQUEEZE details are provided in the CIF file).

2a: The H atoms attached to O1W, O2W (O2W is found at sites of twofold axial symmetry) and O3W were found from difference Fourier maps, and their coordinates were refined freely. The H atoms attached to the lattice water solvent molecules O3W′ (minor component of the disordered water lattice molecule) and O4W [partially occupied with an occupancy factor of 0.292(9)] could not be retrieved from difference Fourier maps. The structure is partly disordered. One part of the Ni complex and one lattice water solvent molecule (O3W/O3W′) is disordered over two orientations, and the occupancy factors of the major components of the disorder refine to 0.649(11) and 0.861(4), respectively. One of the two counterions (Br2) is disordered over three orientations, and the occupancy factors of the three components refine to 0.779(2), 0.180(2) and 0.0410(8).

2b: The structure is ordered, except for some amount of disordered lattice solvent molecules, whose contribution has been taken out using the SQUEEZE procedure[47] in the final refinement (SQUEEZE details are provided in the CIF file).

CCDC 1444939 (for **1a**), 1444940 (for **2a**), and 1444941 (for **2b**) contain the supplementary crystallographic data for this paper. These data can be obtained free of charge from The Cambridge Crystallographic Data Centre.

Electrochemistry: Cyclic voltammetry was recorded with an Autolab PGstat10 potentiostat controlled by GPES4 software under argon. A 3 mm diameter glassy carbon electrode was used as working electrode and a Pt wire as the counter electrode. The experimental reference was an Ag/AgCl electrode in the electrolyte solution (TBAP). Ferrocene was added at the end of each measurement as an internal standard. All electrode potentials reported in this publication are given vs. the potential of the ferrocene/ferrocenium redox couple ([$Fc^{+/0}$], E^o = 0.00 V) as the reference.

Overpotentials were calculated using the following equation:

$$\eta = E^T_{1/2} - E^E_{1/2}$$

Here, $\eta = E^T_{1/2}$ is the thermodynamic standard potential computed in the case of an electrochemically reversible process which considered the homoconjugation effect given by the equation:[44]

$$E^T_{1/2} = E^\circ_{H^+/H_2} = -\frac{2.303 \times RT}{F} pK_a + \varepsilon_D - \frac{RT}{2F} \ln \frac{C_0}{C^\circ_{H_2}}$$

$\eta = E^E_{1/2}$ is the experimental reduction potential, which is defined here as the maximum of the first derivative of the irreversible wave.[44]

The apparent rate constant (k_{obs}) can be regarded as turn-over frequency (TOF) when a first-order or pseudo-first order H_2 evolving reaction is catalyzed by a freely diffusing molecular catalyst.[43] The corresponding equation is provided below:[7,43]

$$\frac{i_c}{i_p} = \frac{n}{0.4463} \sqrt{\frac{RTk_{obs}}{Fv}}$$

Here, i_c is the maximum current of the catalytic peak, and i_p is the plateau current of the non-catalytic reduction wave. F is Faraday's constant, T is 295 K, R is the universal gas constant, v is the scan rate, n is 2 in the case of the H_2 evolution process.

Synthetic Procedures

Synthesis of the Ligands H_2L1Br_2 and H_2L2Br_2: *N*-Pyridylmethyl(benz)imidazole,[28] H_2**L1**Br_2 and H_2**L2**Br_2[29] were synthesized following literature methods with small modifications.

H_2L1Br_2: *N*-Pyridylmethylbenzimidazole (4 mmol, 0.836 g) and α,α′-dibromo-o-xylene (2 mmol, 0.57 g) were added into a 25 mL round-bottomed flask containing 10 mL of toluene. The mixture was stirred for 24 h at 110 °C, after which time the product was collected by filtration. The white powder was washed with THF and ether, and dried under vacuum, yield 1.32g (97 %). ^{1}H NMR (300 MHz, [D_6]DMSO): δ = 10.07 (s, 2 H), 8.48 (d, J = 4.77 Hz, 2 H), 8.04 (s, 1 H), 8.02 (d, J = 3.17 Hz, 2 H), 7.98 (d, J = 2.60 Hz, 1 H), 7.95 (t, J = 2.18, 2.18 Hz, 2 H), 7.92 (d, J = 1.74 Hz, 1 H) 7.90 (d, J = 1.76 Hz, 1 H), 7.74 (s, 1 H), 7.72 (s, 1 H), 7.66 (m, 4 H), 7.44 (dd, J = 3.33, 5.70 Hz, 2 H), 7.38 (dd, J = 5.35, 7.05 Hz, 2 H), 7.19 (dd, J = 3.46, 5.58 Hz, 2 H), 6.16 (s, 2 H), 6.00 (s, 2 H) ppm. ^{13}C NMR (75 MHz, [D_6]DMSO): δ = 152.87, 149.55, 148.05, 143.87, 137.58, 132.06, 131.55, 131.07, 129.37, 128.25, 127.07, 126.80, 123.74, 122.77, 114.07, 50.85, 47.53 ppm. ESI-MS found (calculated): [M – 2Br]$^{2+}$ m/z 261.3 (261.1); [M – Br]$^+$ m/z 601.1 (601.2).

H_2L2Br_2: *N*-Pyridylmethylimidazole (4 mmol, 0.836 g) and α,α′-dibromo-o-xylene (2 mmol, 0.57 g) were added into a 25 mL round-bottomed flask containing 10 mL of toluene. The mixture was stirred for 48 h at 110 °C, after which time the product was collected by filtration. The sticky solid was crushed and washed with THF until it became a brown powder, which was dried under vacuum, yield 0.90 g (76 %). ^{1}H NMR (300 MHz, [D_6]DMSO): δ = 9.48 (s, 2 H), 8.55 (d, 2 H), 7.93 (d, J = 1.5 Hz, 1 H), 7.91 (d, J = 1.2 Hz, 1 H), 7.88 (s, 2 H), 7.82 (s, 2 H), 7.55 (d, J = 8.1 Hz, 2 H), 7.52–7.48 (m, 2 H), 7.41 (dd, J = 4.8, 2.1 Hz, 2 H), 7.32 (dd, J = 3.48, 5.44 Hz, 2 H), 5.73 (s, 4 H), 5.64 (s, 4 H) ppm. ^{13}C NMR (75 MHz, [D_6]DMSO): δ = 153.41, 149.57, 137.54, 137.48, 132.98, 129.64, 129.38, 123.75, 123.70, 122.69, 122.56, 53.09, 49.12 ppm. ESI-MS found (calculated): [M – 2Br]$^{2+}$ m/z 211.2 (211.6); [M – Br]$^+$ m/z 501.0 (502.1).

Synthesis of [Ni(L1)Br]Br (1a) and [Ni(L2)]Br_2 (2a): Tetrabutylammonium bromide (2 g), nickel acetate (0.18 g, 1 mmol) and H_2**L1**Br_2 (0.69 g, 1 mmol) or nickel acetate (0.15 g, 0.84 mmol) and H_2**L2**Br_2 (0.49 g, 0.84 mmol) were weighed into a 10 mL round-bottomed flask. The mixture was heated at 80 °C under vacuum for 3 h. Then the temperature was increased to 120–130 °C and the flask was heated for another 24 h under vacuum. After cooling to room temperature the residue was triturated with 50 mL distilled water, and kept overnight. The mixture was filtered yielding a yellow powder. The powder was thoroughly washed with diethyl ether, yield **1a** 0.55 g (74 %), **2a** 0.29 g (45 %). Single crystals were obtained by the liquid-liquid diffusion method (MeCN/diethyl ether).

1a: ^{1}H NMR (300 MHz, [D_6]DMSO): δ = 8.49 (d, J = 5.50 Hz, 2 H), 8.13 (m, 6 H), 7.885 (dd, J = 3.66, 5.20 Hz, 2 H), 7.34–7.44 (m, 10 H), 7.25 (t, J = 7.70, 7.70 Hz, 2 H), 6.465 (d, J = 15.22 Hz, 2 H), 5.45 (d,

J = 16.06 Hz, 2 H), 5.32 (d, J = 15.93 Hz, 2 H) ppm. ^{13}C NMR (75 MHz, [D$_6$]DMSO): δ = 168.43, 154.56, 153.16, 141.00, 134.30, 134.04, 132.86, 132.78, 128.81, 124.81, 124.64, 124.34, 124.04, 112.77, 111.35, 50.76, 50.12 ppm. ESI-MS found (calculated): [M – 2Br]$^{2+}$ m/z 289.0 (289.1); [M – Br]$^+$ m/z 657.1 (657.1). $C_{34}H_{28}Br_2N_6Ni$ (739.15): calcd. C 55.25, H 3.82, N 11.37; found C 54.57, H 3.93, N 11.80.

2a: ^{1}H NMR (300 MHz, [D$_6$]DMSO): δ = 8.30 (d, J = 5.27 Hz, 2 H), 8.11 (t, J = 7.62, 7.62 Hz, 2 H), 7.88 (d, J = 7.62 Hz, 2 H), 7.71 (d, J = 1.56 Hz, 2 H), 7.55 (m, 2 H), 7.35–7.37 (m, 4 H), 6.98 (m, 4 H), 5.81 (d, J = 14.99 Hz, 2 H), 5.01 (d, J = 15.46 Hz, 2 H), 4.69 (d, J = 15.30 Hz, 2 H) ppm. ^{13}C NMR (75 MHz, DMSO): δ = 155.56, 154.67, 152.64, 140.83, 135.54, 131.42, 129.04, 124.97, 124.84, 124.67, 122.80, 53.39, 51.50 ppm. ESI-MS found (calculated): [M – 2Br]$^{2+}$ m/z 239.1 (239.1); [M – Br]$^+$ m/z 557.0 (557.1). $C_{26}H_{24}Br_2N_6Ni{\cdot}H_2O$: calcd. C 47.53, H 3.99, N 12.79; found C 47.73, H 3.74, N 12.69.

Synthesis of [Ni(L1)](PF$_6$)$_2$ (1b) and [Ni(L$_2$)](PF$_6$)$_2$ (2b): NH_4PF_6 (128 mg, 0.4 mmol) was dissolved in 15 mL of methanol and the solution was brought to a boil. The compounds **1a** (74 mg, 0.1 mmol) or **2a** (64 mg, 0.1 mmol) were added into this boiling methanol solution. The resulting suspension was stirred for 30 min during which time it cooled down. The product was collected by filtration and the pale yellow solid was washed with cold methanol and diethyl ether, yield **1b** 35 mg (55 %), **2b** 55 mg (72 %). Single crystals were obtained by the liquid-liquid diffusion method (MeCN/diethyl ether).

1b: ^{1}H NMR (300 MHz, [D$_6$]DMSO): δ = 8.42 (s, J = 5.26 Hz, 2 H), 8.15–8.18 (m, 5 H), 7.87 (dd, J = 3.61, 5.23 Hz, 2 H), 7.40–7.46 (m, 6 H), 7.37 (s, 1 H), 7.27 (m, 2 H), 7.02 (d, J = 15.23 Hz, 2 H), 6.43 (d, J = 15.32 Hz, 2 H), 5.48 (d, J = 15.99 Hz, 2 H), 5.17 (d, J = 15.83 Hz, 2 H) ppm. ^{13}C NMR (75 MHz, [D$_6$]DMSO): δ = 168.11, 154.54, 152.65, 141.23, 134.23, 132.89, 132.76, 128.82, 124.97, 124.89, 124.40, 124.06, 112.86, 111.42, 101.22, 50.41, 49.89 ppm. ^{31}P NMR (122 MHz, [D$_6$]DMSO): δ = –144.88 ppm. ESI-MS found (calculated): [M – 2PF$_6$]$^{2+}$ m/z 289.9 (289.9); [M – PF$_6$]$^+$ m/z 723.2 (723.1). $C_{34}H_{28}N_6Ni(PF_6)_2{\cdot}CH_3CN$: calcd. C 47.50, H 3.43, N 10.77; found C 47.78, H 3.43, N 10.80.

2b: ^{1}H NMR (300 MHz, [D$_6$]DMSO): δ = 8.25 (d, J = 15.99 Hz, 2 H), 8.12 (t, J = 7.41, 7.41 Hz, 2 H), 7.89 (d, J = 7.57 Hz, 2 H), 7.71 (s, 2 H), 7.54 (m, 2 H), 7.40–7.46 (m, 4 H), 6.99 (s, 2 H), 6.77 (d, J = 14.93 Hz, 2 H), 5.80 (d, J = 15.01 Hz, 2 H), 5.04 (d, J = 15.39 Hz, 2 H), 4.61 (d, J = 15.26 Hz, 2 H) ppm. ^{13}C NMR (75 MHz, [D$_6$]DMSO): δ = 155.45, 154.62, 152.33, 141.01, 135.47, 131.44, 129.10, 125.17, 124.99, 124.88, 122.93, 53.28, 51.34 ppm. ^{31}P NMR (122 MHz, [D$_6$]DMSO): δ = –144.87 ppm. ESI-MS found (calculated): [M – 2PF$_6$]$^{2+}$ m/z 239.1 (239.6). $C_{26}H_{24}N_6Ni(PF_6)_2$: calcd. C 40.60, H 3.15, N 10.93; found C 40.64, H 3.18, N 10.92.

Acknowledgments

S. L. gratefully acknowledges a grant from the Chinese Scholarship Council (grant number 201306410011). The authors are grateful to Mr. John van Dijk for mass spectrometry.

Keywords: *N*-Heterocyclic carbenes · Carbenes · Nickel · Cyclic voltammetry · Electrocatalysis · Proton reduction

[1] P. D. Tran, J. Barber, *Phys. Chem. Chem. Phys.* **2012**, *14*, 13772–13784.
[2] J. D. Holladay, J. Hu, D. L. King, Y. Wang, *Catal. Today* **2009**, *139*, 244–260.
[3] V. Khrizanforova, I. Knyazeva, V. Matveeva Sokolova, I. Nizameev, T. Gryaznova, M. Kadirov, A. Burilov, O. Sinyashin, Y. Budnikova, *Electrocatalysis* **2015**, *6*, 357–364.
[4] A. Lewandowska-Andralojc, T. Baine, X. Zhao, J. T. Muckerman, E. Fujita, D. E. Polyansky, *Inorg. Chem.* **2015**, *54*, 4310–4321.
[5] N. Queyriaux, R. T. Jane, J. Massin, V. Artero, M. Chavarot-Kerlidou, *Coord. Chem. Rev.* **2015**, *304–305*, 3–19.
[6] S. Canaguier, V. Fourmond, C. U. Perotto, J. Fize, J. Pecaut, M. Fontecave, M. J. Field, V. Artero, *Chem. Commun.* **2013**, *49*, 5004–5006.
[7] L. Gan, T. L. Groy, P. Tarakeshwar, S. K. S. Mazinani, J. Shearer, V. Mujica, A. K. Jones, *J. Am. Chem. Soc.* **2015**, *137*, 1109–1115.
[8] D. L. DuBois, R. M. Bullock, *Eur. J. Inorg. Chem.* **2011**, 1017–1027.
[9] M. T. M. Koper, E. Bouwman, *Angew. Chem. Int. Ed.* **2010**, *49*, 3723–3725; *Angew. Chem.* **2010**, *122*, 3810.
[10] S. M. Laga, J. D. Blakemore, L. M. Henling, B. S. Brunschwig, H. B. Gray, *Inorg. Chem.* **2014**, *53*, 12668–12670.
[11] L. Tong, R. Zong, R. P. Thummel, *J. Am. Chem. Soc.* **2014**, *136*, 4881–4884.
[12] D. Basu, S. Mazumder, X. Shi, H. Baydoun, J. Niklas, O. Poluektov, H. B. Schlegel, C. N. Verani, *Angew. Chem. Int. Ed.* **2015**, *54*, 2105–2110; *Angew. Chem.* **2015**, *127*, 2133.
[13] R. M. Stolley, J. M. Darmon, M. L. Helm, *Chem. Commun.* **2014**, *50*, 3681–3684.
[14] M. van der Meer, E. Glais, I. Siewert, B. Sarkar, *Angew. Chem. Int. Ed.* **2015**, *54*, 13792–13795; *Angew. Chem.* **2015**, *127*, 13997.
[15] J. Berding, T. F. van Dijkman, M. Lutz, A. L. Spek, E. Bouwman, *Dalton Trans.* **2009**, 6948–6955.
[16] L. P. Bheeter, M. Henrion, L. Brelot, C. Darcel, M. J. Chetcuti, J.-B. Sortais, V. Ritleng, *Adv. Synth. Catal.* **2012**, *354*, 2619–2624.
[17] E. A. Bielinski, W. Dai, L. M. Guard, N. Hazari, M. K. Takase, *Organometallics* **2013**, *32*, 4025–4037.
[18] K. Fuji, S. Tamba, K. Shono, A. Sugie, A. Mori, *J. Am. Chem. Soc.* **2013**, *135*, 12208–12211.
[19] P. Guan, C. Cao, Y. Liu, Y. Li, P. He, Q. Chen, G. Liu, Y. Shi, *Tetrahedron Lett.* **2012**, *53*, 5987–5992.
[20] L. Postigo, B. Royo, *Adv. Synth. Catal.* **2012**, *354*, 2613–2618.
[21] Z. Xi, X. Zhang, W. Chen, S. Fu, D. Wang, *Organometallics* **2007**, *26*, 6636–6642.
[22] Z. Xi, B. Liu, W. Chen, *J. Org. Chem.* **2008**, *73*, 3954–3957.
[23] M. C. Jahnke, T. Pape, F. E. Hahn, *Eur. J. Inorg. Chem.* **2009**, 1960–1969.
[24] M. H. Reineke, M. D. Sampson, A. L. Rheingold, C. P. Kubiak, *Inorg. Chem.* **2015**, *54*, 3211–3217.
[25] V. S. Thoi, C. J. Chang, *Chem. Commun.* **2011**, *47*, 6578–6580.
[26] V. S. Thoi, N. Kornienko, C. G. Margarit, P. Yang, C. J. Chang, *J. Am. Chem. Soc.* **2013**, *135*, 14413–14424.
[27] Q.-X. Liu, Z.-Q. Yao, X.-J. Zhao, Z.-X. Zhao, X.-G. Wang, *Organometallics* **2013**, *32*, 3493–3501.
[28] J. Dinda, S. D. Adhikary, S. K. Seth, A. Mahapatra, *New J. Chem.* **2013**, *37*, 431–438.
[29] J. Berding, M. Lutz, A. L. Spek, E. Bouwman, *Organometallics* **2009**, *28*, 1845–1854.
[30] A. W. Addison, T. N. Rao, J. Reedijk, J. Vanrijn, G. C. Verschoor, *J. Chem. Soc., Dalton Trans.* **1984**, 1349–1356.
[31] R. García-Bueno, M. D. Santana, G. Sanchez, J. Garcia, G. Garcia, J. Perez, L. Garcia, *Dalton Trans.* **2010**, *39*, 5728–5736.
[32] E. I. Musina, V. V. Khrizanforova, I. D. Strelnik, M. I. Valitov, Y. S. Spiridonova, D. B. Krivolapov, I. A. Litvinov, M. K. Kadirov, P. Lonnecke, E. Hey-Hawkins, Y. H. Budnikova, A. A. Karasik, O. G. Sinyashin, *Chemistry* **2014**, *20*, 3169–3182.
[33] M. D. Santana, A. A. Lozano, G. Garcia, G. Lopez, J. Perez, *Dalton Trans.* **2005**, 104–109.
[34] H. Ma, S. Chattopadhyay, J. L. Petersen, M. P. Jensen, *Inorg. Chem.* **2008**, *47*, 7966–7968.
[35] H. Ma, J. L. Petersen, V. G. Young, G. T. Yee, M. P. Jensen, *J. Am. Chem. Soc.* **2011**, *133*, 5644–5647.
[36] S. F. Tyler, S. N. Natoli, B. Vlaisavljevich, P. E. Fanwick, T. Ren, *Inorg. Chem.* **2015**, *54*, 10058–10064.
[37] J.-i. Nishigaki, T. Matsumoto, K. Tatsumi, *Eur. J. Inorg. Chem.* **2010**, 5011–5017.
[38] L. Yang, D. R. Powell, R. P. Houser, *Dalton Trans.* **2007**, 955–964.

[39] E. C. M. Ording-Wenker, M. A. Siegler, M. Lutz, E. Bouwman, *Inorg. Chem.* **2013**, *52*, 13113–13122.
[40] M. Sheng, N. Jiang, S. Gustafson, B. You, D. H. Ess, Y. Sun, *Dalton Trans.* **2015**, *44*, 16247–16250.
[41] J. Heinze, *Angew. Chem. Int. Ed. Engl.* **1984**, *23*, 831–847; *Angew. Chem.* **1984**, *96*, 823.
[42] V. Fourmond, S. Canaguier, B. Golly, M. J. Field, M. Fontecave, V. Artero, *Energy Environ. Sci.* **2011**, *4*, 2417–2427.
[43] P. Zhang, M. Wang, Y. Yang, T. Yao, L. Sun, *Angew. Chem. Int. Ed.* **2014**, *53*, 13803–13807; *Angew. Chem.* **2014**, *126*, 14023.
[44] V. Fourmond, P.-A. Jacques, M. Fontecave, V. Artero, *Inorg. Chem.* **2010**, *49*, 10338–10347.
[45] K. Kawano, K. Yamauchi, K. Sakai, *Chem. Commun.* **2014**, *50*, 9872–9875.
[46] G. M. Sheldrick, *Acta Crystallogr., Sect. A: Found. Crystallogr.* **2008**, *64*, 112–122.
[47] A. L. Spek, *Acta Crystallogr., Sect. D Biol. Crystallogr.* **2009**, *65*, 148–155.

Received: July 25, 2016
Published Online: August 29, 2016